

MOFs Modified Paper-Based Materials: Preparation and Application to EtOH Fluorescence Response

¹Qiang Yang*, ²Meiyun Zhang, ¹Wei Gong, ¹Xiaowei Cui, ¹Chunsheng Zhou

¹College of Chemical Engineering and Modern Materials, Shaanxi Key Laboratory of Comprehensive Utilization of Tailings Resources, Shangluo University, Shangluo 726000, Shaanxi Province, P.R. China.

²Shaanxi Provincial Key Laboratory of Papermaking Technology and Specialty Paper Development, Key Laboratory of Paper Based Functional Materials of China National Light Industry, College of Bioresources Chemical and Materials Engineering, Shaanxi University of Science and Technology, Xi'an 710021, Shaanxi Province, P.R. China.

yq_sust@163.com*

(Received on 19th May 2021, accepted in revised form 30th November 2021)

Summary: Based on the solvothermal method, two new MOFs with 3-(1-Oxo-1H-2,3-dihydroisoindol-2-yl)benzoic acid as the organic ligand, Zn-HBPA and Zn-bpy-HBPA were synthesized. The structure of MOFs was characterized by ¹H-NMR, XRD, FT-IR and SEM. A series of modified cellulose paper-based functional materials with different spraying times were prepared by flame spraying method, and the fluorescence property of MOFs modified cellulose paper to EtOH small molecules was investigated by fluorescence spectrometer. The results of FT-IR and SEM showed that the flame spraying method could effectively improve the retention rate of MOFs on cellulose paper materials. The PL characterization results displayed that Zn-HBPA@PFP exhibited a decrease in fluorescence after UV irradiation, while Zn-bpy-HBPA@PFP demonstrated an increase in fluorescence at $\lambda=338$ nm. The above results indicated that Zn-bpy-HBPA@PFP had an excellent response ability to EtOH small molecules, and when Cycle=7 times, Zn-bpy-HBPA@PFP had the best fluorescence enhancement effect.

Keywords: Flame spraying; MOFs; Cellulose Paper; Fluorescence response.

Introduction

The design and synthesis of Metal Organic Frameworks (MOFs) have received extensive attention. MOFs were under a wide range of applications in gas adsorption, ion exchange, chemical separation, nonlinear optics, heterogeneous catalysis, and properties of modifiable and diverse topological structures had research potential. [1-4]. At this stage, metals based on the d^{10} structure had excellent light-emitting functions and potential applications in light-emitting diodes have become a research focus. [5,6] The factors affecting the luminescence performance of coordination chemicals mainly include: temperature, metal ions and solvent systems, etc. [7,8] However, the fluorescence performance had the phenomenon of Aggregation-Caused Quenching (ACQ), [9] it was usually weakened or quenched at high concentrations or in a solid state, which made it impossible to detect and characterize. Hu *et al.* (2014) [10] and Shuastova *et al.* (2012) [11] proposed to constructing fluorescent luminophores inside MOFs to achieve the purpose of fluorescence emission. In this work, the fluorescence properties of a rigid ligand based on N-substituted aromatic and MOF(Zn) were recorded.

Research by Yang *et al.* (2014) [12] showed

that the luminescence mechanism of aromatic compounds related to their conjugation effect, the orbital transition from π to π^* or π to n . In addition, Sun *et al.* (2007) [13] reported that a ligand with a large π -conjugation effect system could improve the luminescence properties of the compound. Although there were many reports on the use of simple and rigid aromatic carboxylic acids such as terephthalic acid, trimesic acid, and pyromellitic acid as ligands, however, few reports on ligands of its derivatives. [14-16] Based on the above considerations, a new ligand 3-(1-Oxo-1H-2,3-dihydroisoindol-2-yl)benzoic acid (HBPA) was introduced, due to construct a new MOFs structure. HBPA had a large rigid π -conjugated system that contains aromatic substituents coplanar with the benzene ring, which could enhance and stabilize the delocalized state of the potential luminescent ligand-ligand transfer (LLCT) and reduce the energy gap. The advantages of HBPA were: 1) HBPA had convenient coordination carboxyl and oxygen groups, which provided coordination sites during the formation of MOFs; 2) HBPA had a similar structure to isophthalic acid, which considered that a carboxyl group of isophthalic acid was replaced by a macrocyclic molecule. Therefore, the substituents could bend or

*To whom all correspondence should be addressed.

distort the plane of the benzene ring, and ultimately promote molecular isomerization through conformational diversity; 3) The oxygen substituents in HBPA acted as hydrogen bond acceptors, and the adjacent C-H bonds acted as hydrogen bond donors, which could further form an intramolecular hydrogen bond network.

Experimental

Materials

O-phthalaldehyde (OPA), 5-Aminoisophthalic acid were of analytical reagent grade from J&K Co., Ltd. (Shanghai China). 2,2'-dipyridyl, 1,4-benzenedicarboxylic acid (H₂BDC), Zn(NO₃)₂·6H₂O, *N,N*-dimethylformamide (DMF) was obtained from KeLong Chemical Co., Ltd. (Chengdu China). Absolute ethyl alcohol (EtOH), ethyl acetate, sodium bicarbonate (NaHCO₃) and acetone was supplied by DaMao Chemical Co., Ltd. (Tianjing China). The retention aid, cationic polyacrylamide (CPAM) was provided by Nalco Chemical Company, Nanjing, China. The bleached hardwood kraft pulp were offered by a paper mill in Shandong, China. The pulp was refined to 40° SR using a PFI refiner. All above chemicals were used without further purification.

Preparation of 3-(1-Oxo-1H-2,3-dihydroisoindol-2-yl) benzoic acid (HBPA)

The preparation scheme was shown in Fig. 1, and the specific steps were as follows: 5 mmol OPA and 5 mmol 5-aminoisophthalic acid was slowly dissolved in 60 mL of a mixed solution of acetone and deionized water ($V_{\text{acetone}} : V_{\text{H}_2\text{O}} = 1:5$), and reflux at 110°C for 3h. The above system was cooled to room temperature, after suction filtration, washed with deionized water several times to neutrality, and then purified with ethyl acetate, recrystallized with EtOH, dried in vacuum at 50°C for 6 hours to obtain a brown-black product for use.

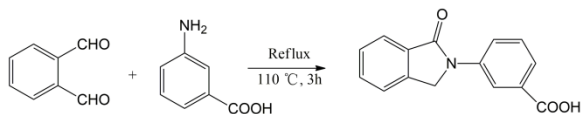


Fig. 1: The synthesis procedure of HBPA

Preparation of Zn-HBPA and Zn-bpy-HBPA

1mmol H₂BDC and 1mmol HBPA was

dissolved in 20 mL DMF/EtOH ($V_{\text{DMF}}:V_{\text{EtOH}}=5:3$) mixture solution at room temperature, and 0.5 mol NaHCO₃ solution was added to adjust the pH to 9.5. The above reaction system was quickly moved into a Teflon reactor, and reacted at 140°C for 8 hours. After slowly cooling to room temperature, it was washed 5 times with DMF and absolute ethanol. Baked in a vacuum drying oven at 50°C for 4 hours, the obtained product was labeled Zn-HBPA.

1mmol H₂BDC, 1mmol HBPA and 0.156 g bpy was dissolved in 20 mL DMF/EtOH mixture solution at room temperature. Then a few drops of deionized water were added to adjust the pH to 7.5. The above reaction system was soon moved into the reaction kettle, and reacted for 8 hours at 140°C. After slowly cooling to room temperature, it was washed 5 times with DMF and absolute ethanol. Baked in a vacuum drying oven at 50°C for 4 hours, and the obtained product was marked as Zn-bpy-HBPA.

Preparation of cellulose paper (PFP)

PFP handsheets preparation procedure referred to Tappi standard T205sp—95. 12 g absolutely dry fiber pulp board was decomposed and dispersed in a decomposer at a concentration of 1.2%, and diluted with water to a concentration of 0.5%. The quantitative control of handsheets was 65 g/m². During the papermaking process, 0.02% CPAM was added to the fiber dispersion system to disperse on a circular sheet former, and then dried at 105±2 °C for 5 min.

Preparation of Zn-HBPA@PFP and Zn-bpy-HBPA@PFP

The preparation scheme was shown in Fig. 2, Zn-HBPA@PFP and Zn-bpy-HBPA@PFP were prepared by flame spraying method. Place the pre-cut PFP paper strips (2×5 cm) in a 10×20 cm glass container, spray them several times (1/3/5/7/9/12), and dry them naturally at room temperature, marked as (Cycle 1, Cycle 3, Cycle 5, Cycle7, Cycle9, Cycle 12). Since the pore size between the fiber and fiber of cellulose paper was 2~10 μm, when the MOFs/EtOH mixture was directly coated on the surface of the paper by the coating method, most of the MOFs would be lost as the EtOH flowed between the fiber holes, which ultimately lead to poor fluorescence performance. Spraying method was used to spray MOFs on the surface of the paper, which had the advantages of improving retention, preventing loss, and not affecting the performance of composite materials.

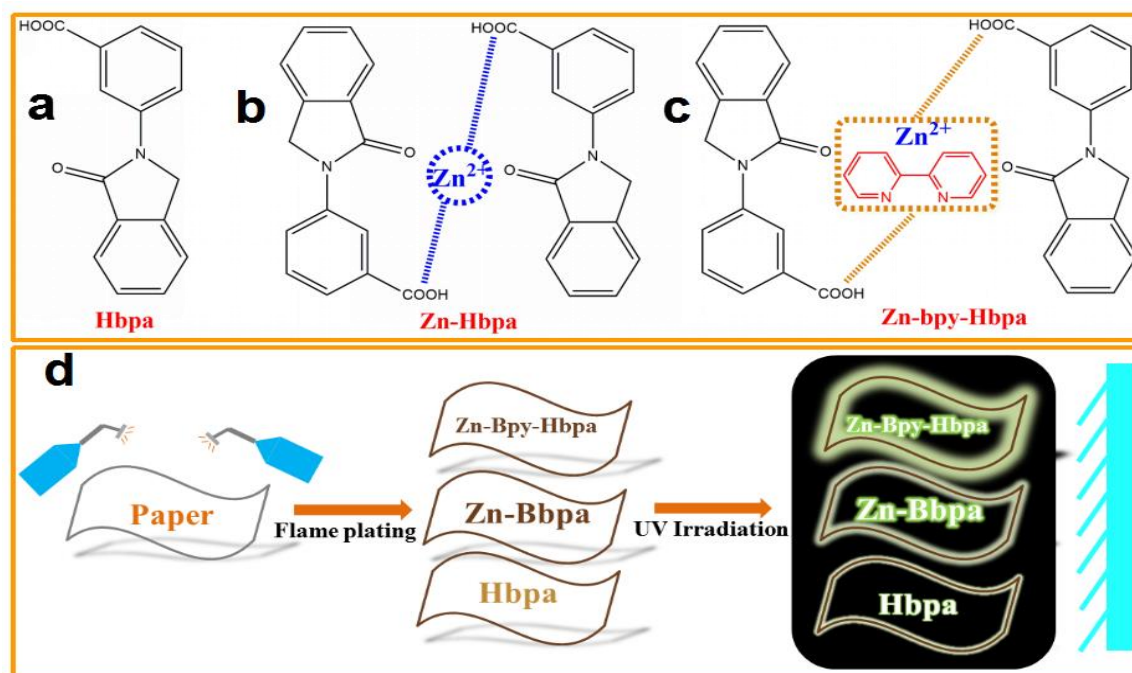


Fig. 2: The schematic of the concept of preparing HBPA, Zn-HBPA, Zn-bpy-HBPA composited with cellulose paper (Structure of (a) HBPA; (b) Zn-HBPA; (c) Zn-bpy-HBPA; (d) preparing procedure).

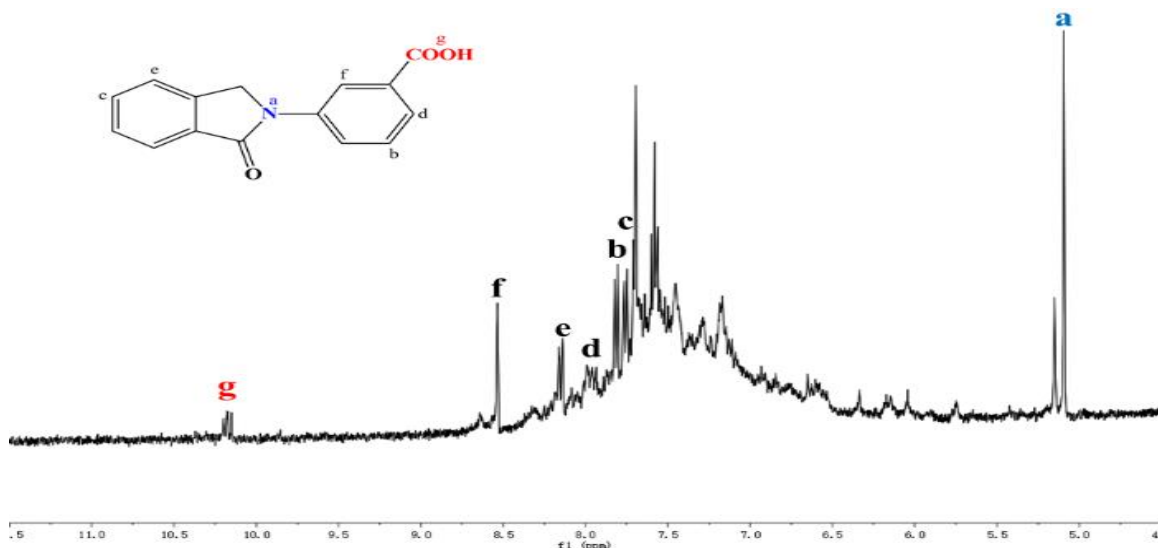


Fig. 3: ¹H-NMR spectra of 3-(1-Oxo-1H-2,3-dihydroisoindol-2-yl)benzoic acid.

Characteristic analysis

The ¹H-Nuclear Magnetic Resonance spectra (NMR) of HBPA powder were recorded on a Bruker Advanced III with DMSO-d₆. The attenuated total reflection-Fourier transform infrared spectroscopy (ATR-FTIR) spectra of all samples were displayed by a Bruker Victory 22, accumulating 32 scans from 400 to 4000 cm⁻¹ with a resolution of 4 cm⁻¹. The X-ray

diffraction (XRD) patterns of the samples were generated using a D/max 2200PC X-ray diffractometer (40 kV, 20 mA) with a Cu Kα (k = 0.1542 nm) anode from 5° to 60° with a 0.025°/s step. The surface morphology and cross section of the samples which were coated with Pt, were characterized with a HITACHI-S4800 Scanning Electron Microscope. Fluorescence spectroscopy spectrums of MOFs@cellulose paper response to small molecules

of EtOH under different spraying times were detected with a Fluoro-4P.

Results and discussion

¹H-NMR Spectra Analysis of HBPA

Fig 3 was the ¹H-NMR spectrum of the organic ligand HBPA, using DMSO-d₆ (δ=2.50 ppm shift) as the solvent for the sample, the chemical shift of each peak of HBPA was analyzed, as follows, HBPA (δ, ppm, DMSO-d₆): 5.10 (s, 2H), 7.70 (m, 2H), 7.60 (m, 2H), 7.81 (s, 2H), 8.16 (s, 1H), 8.50 (s, 1H), 11.0 (s, 1H). The above analysis showed that molecular structure of HBPA contains rigid benzene ring structure, N-substituted five-membered ring, carboxyl group, etc., indicated that the NDI sample had been successfully prepared. Chen *et al.* (2013) [17] used different methods to prepare 2-(1-oxo-1*H*-2,3-dihydroisindol-2-yl, oHBPA) benzoic acid, and discussed its structure. The results showed that oHBPA had a layered stacked structure, and the O—H—C (aryl) of a single layer molecules formed a 3-D hydrogen bond network structure through hydrogen bonding, while mHBPA had a planar structure of a "head-to-head" orientation between the molecules. oHBPA molecules were linked by O(COO)—H—O(COO) hydrogen bonds to constitute a 2-D planar structure.

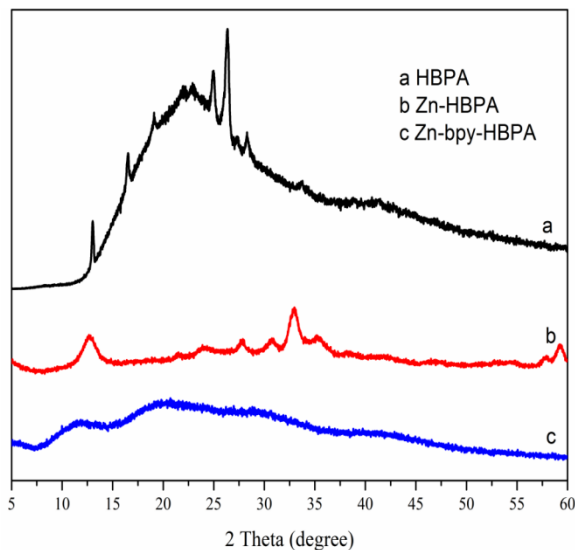


Fig. 4: The XRD curves of HBPA, Zn-HBPA and Zn-bpy-HBPA.

XRD Spectrum Analysis

XRD was utilized to characterize HBPA, Zn-HBPA, Zn-bpy-HBPA. As shown in Fig. 4, the diffraction peaks at $2\theta=12.5^\circ$, 23.5° , and 27.5° were attributed to the characteristic diffraction peaks of HBPA, after the formation of Zn-HBPA, the above described characteristic peaks still could be found. Meanwhile, new diffraction peaks were found at $2\theta=22^\circ$, 31.5° , and 33° , indicated that Zn (II) was coordinated with the HBPA. Ye *et al.* (2015) [18] synthesized H₂IDPA based on trimellitic acid, and found similar research results after it was coordinated with Cd. In addition, as Fig 4 described, the absorption peaks of Zn-bpy-HBPA formed by doping 2,2'-bipyridine became weaker, and it only showed obvious diffraction peaks around $2\theta=12.5^\circ$, 20.5° , 28.5° . The reason was that the Zn-bpy structure was formed through the interaction of $\pi\cdots\pi$ and $\text{CH}\cdots\pi$. The Zn-bpy chains was further immobilized between two negatively charged framework metal clusters, resulting in defects in the crystal structure of Zn-bpy-HBPA, which was manifested by the weakening of its XRD diffraction peaks.

FT-IR Spectrum Analysis

The infrared absorption peaks of HBPA@PFP, Zn-HBPA@PFP, Zn-bpy-HBPA@PFP were illustrated in Fig 5. 3421 cm^{-1} was the vibration peak of -OH-, 3050 cm^{-1} was the vibration peak of the aromatic ring, 2906 cm^{-1} , 2820 cm^{-1} were the antisymmetric stretching and symmetrical stretching vibration peaks of the methylene group in the aromatic ring. In addition, due to the conjugation between the benzene ring, carboxyl group and sp^2 heterocyclic nitrogen, the characteristic stretching vibration absorption peak of carbonyl lactam was red-shifted to around 1654 cm^{-1} , free carboxyl peaks could be found near 1365 cm^{-1} and 1300 cm^{-1} . However, the absorption peaks at 1595 cm^{-1} and 1433 cm^{-1} were attributed to the skeleton vibration peaks of the aromatic ring. The characteristic peaks at 758 cm^{-1} and 685 cm^{-1} were attributed to the -C-H- out-of-plane bending vibration peaks on the meta-substituted benzene ring. The characteristic peak near 474 cm^{-1} was the characteristic stretching vibration peak of -Zn-O-, and the characteristic absorption peak near 1160 cm^{-1} was the characteristic absorption peak of the fiber. The above results suggested that two MOFs with HBPA as the organic ligand was formed and successfully combined into pure fiber paper.

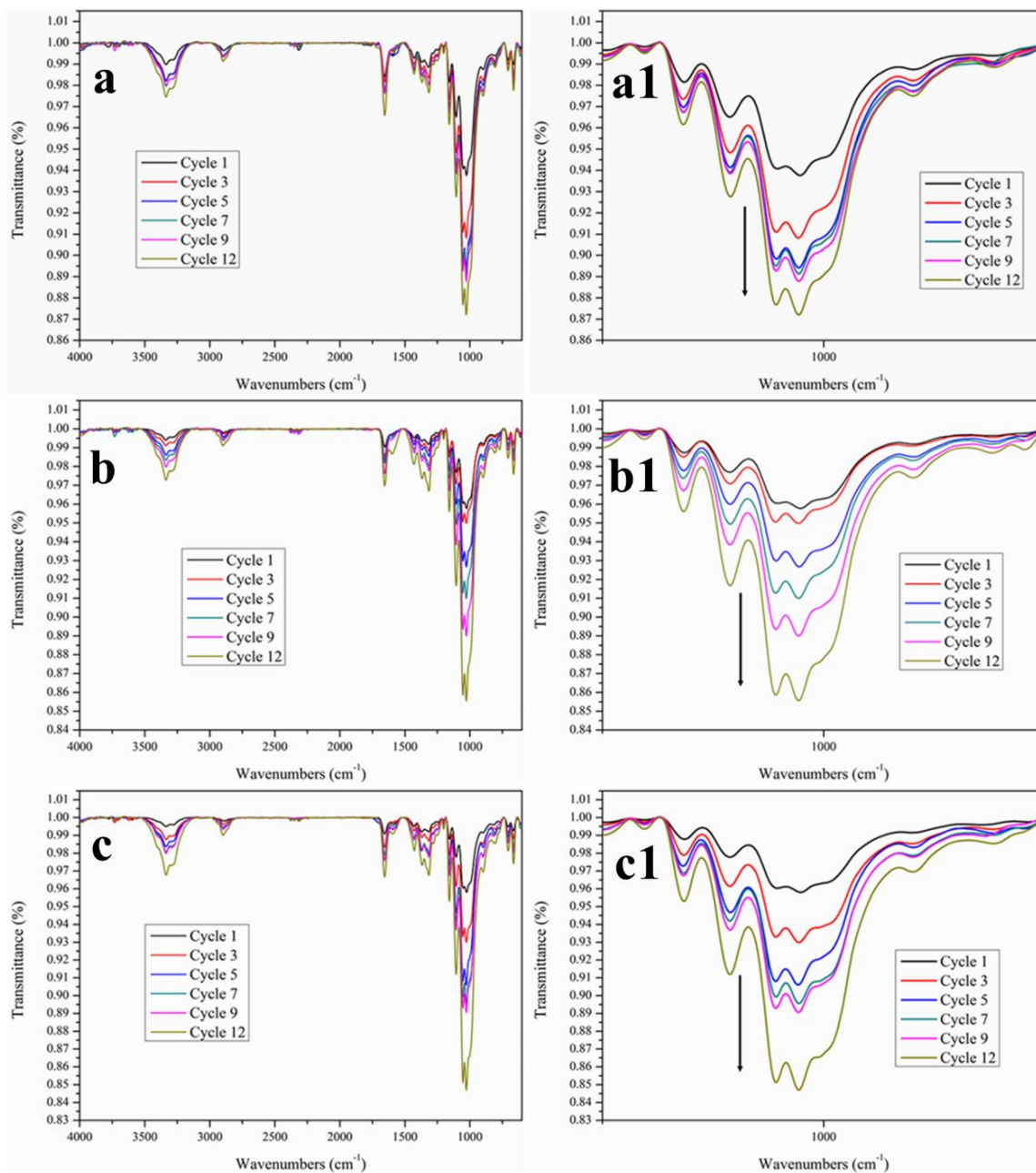


Fig. 5: The FT-IR spectrum of (a) HBPA@PFP, (b) Zn-HBPA@PFP and (c) Zn-bpy-HBPA@PFP.

Furthermore, after inspecting different spray times (Cycle1, Cycle3, Cycle5, Cycle7, Cycle9, Cycle12), the infrared absorption of the paper-based composite material was analyzed (Fig. a1, b1, c1). As demonstrated to Fig. 5, it could be found that with the increase of spraying times, the infrared absorption around 1000 cm⁻¹ showed a regular change, indicating that as the spraying times increase, the infrared absorption becomes stronger, when Cycle=12 times, the transmission intensity rate of samples reached the maximum.

SEM Morphology Analysis

Fig. 6 displayed the SEM images of HBPA, Zn-HBPA, Zn-bpy-HBPA and MOFs@PFP samples under different spraying times. As shown in Fig 6a and 6b, the prepared HBPA particles presented a regular geometric shape, showing the easy agglomeration characteristics of nanoparticles due to the size effect. In one-dimensional direction, the average size of HBPA were about 40~120 nm. After the formation of Zn-HBPA with Zn(NO₃)₂·6H₂O through coordination,

it could be clearly seen in the high-magnification image that Zn-HBPA presents a regular flake shape (Fig 6d), with an average size of 200~500 nm. Compared with HBPA and Zn-HBPA, under the same

synthesis conditions, Zn-bpy-HBPA prepared by introducing bpy that had a hollow spherical shape with a size distribution in the range of 2 μm (Fig f).

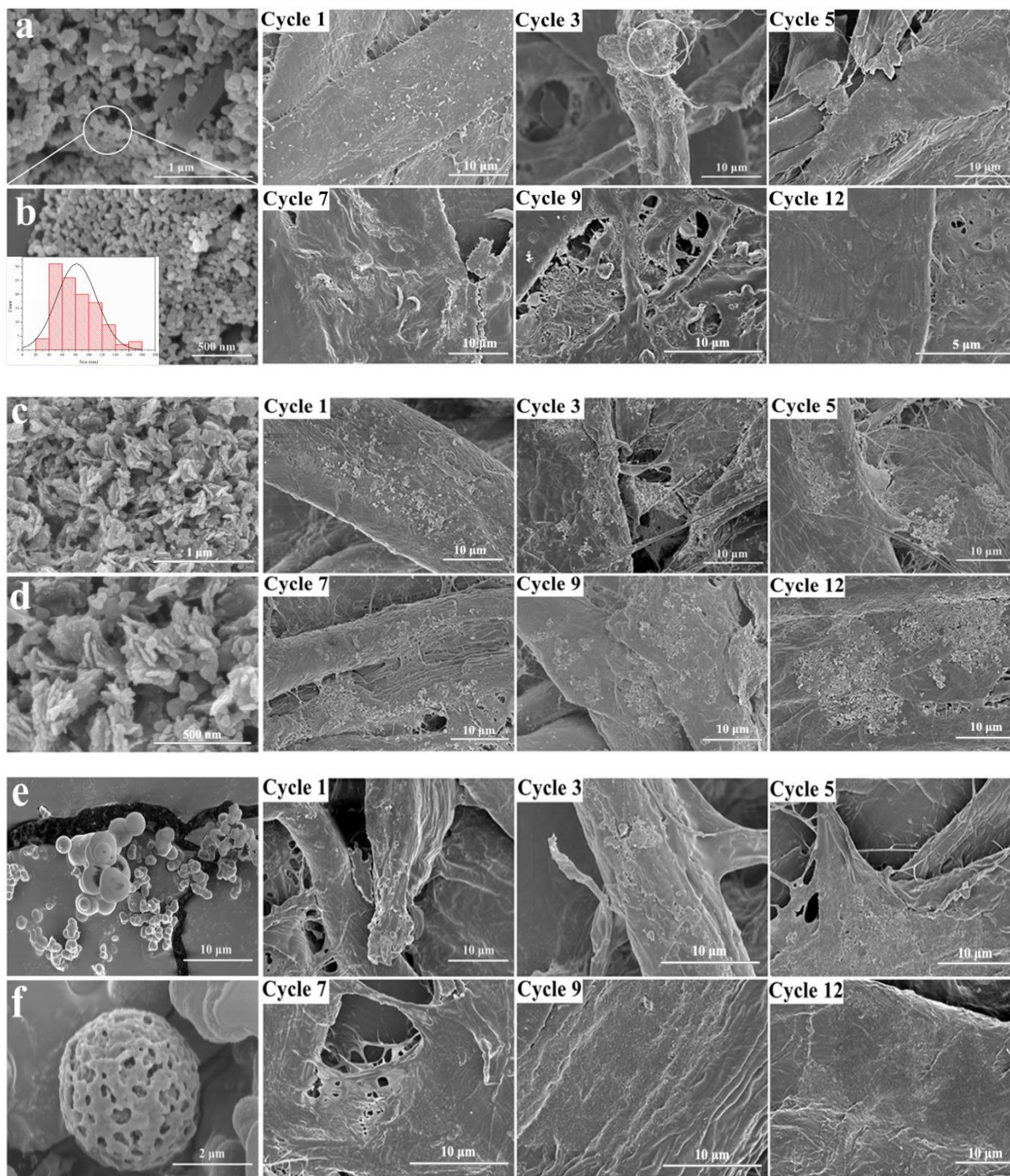


Fig. 6: SEM images of (a,b) HBPA; (c,d) Zn-HBPA; (e,f) Zn-bpy-HBPA and their modified cellulose paper-based functional materials with different spray times.

On this basis, the micro morphology of the paper-based composites under different spraying times (Cycle 1, Cycle 3, Cycle 5, Cycle 7, Cycle 9, Cycle 12) were investigated. As the number of spraying times increased, the retention of nanoparticles on the surface of the composite material gradually increases. When Cycle=12 times, the particle retention effect on the surface of the three paper-based composite materials reached the maximum, which also corroborates the results of FT-IR data analysis.

Fluorescence property of MOFs@PFP to EtOH Small Molecules

Zn²⁺ had a d¹⁰ electronic structure which electron structure layer which did not contain unpaired electrons. Besides, Zn²⁺ could form complexes with aromatic organic ligands with large conjugated π bonds. Therefore, MOFs with Zn²⁺ as the metal center could generally produce photoluminescence based on their corresponding organic ligands. In this work, flame spraying method was used to spray pure fiber paper in different times to prepare MOFs@PFP composite material, and perform fluorescence spectroscopy (PL) test. Taking into consideration the interaction between EtOH small molecules and the hydrogen bonds between MOFs frameworks, it is expected that a flexible paper-based functional material with fluorescence responsiveness to EtOH small molecules can be obtained.

Figs 7a and 7b were the fluorescence excitation emission spectra of Zn-HBPA@PFP and Zn-bpy-HBPA@PFP under different spraying times. The excitation wavelengths were $\lambda=442$ nm and $\lambda=436$ nm, respectively. Among them, Zn-HBPA@PFP emitted blue light at $\lambda=337$ nm, and Zn-bpy-HBPA@PFP emitted blue light at $\lambda=338$ nm. The mechanism of blue light emission lied in the charge transfer (LMCT) of the ligand—metal ion bond. In addition, Figs 7c and 7d were the excitation emission spectra of Zn-HBPA@PFP and Zn-bpy-HBPA@PFP in response to EtOH small molecules under different spraying times. It could be obviously seen from that the luminous intensity of the above two paper-based functional materials changes significantly after responding to the EtOH molecule. The luminous intensity of Zn-HBPA@Paper was weakened, which was reflected as a phenomenon of reduced fluorescence, while the luminous intensity of Zn-bpy-HBPA@PFP was increased, which was manifested as a phenomenon of increased fluorescence. The reason for the difference in the above phenomenon was that after Zn-HBPA contacted EtOH, an EtOH-(Zn-HBPA)

structure containing hydrogen bonds was established. Under the excitation of ultraviolet light, the internal conversion process and the luminescence process competed with each other. Barman *et al.* (2013) [19] pointed out that the hydrogen bond had a positive effect on adjusting the energy levels of the various electronic states of the system. Whenever a new hydrogen bond system was formed, its energy level will drop, and as the strength of the hydrogen bond was formed, the energy level will drop more. The EtOH small molecule formed a certain interaction with the organic ligand HBPA formed by N substitution, which increased the strength of the hydrogen bond, and promoted the coupling vibration of CO, NH, and OH, which increased the non-radiative energy attenuation of MOFs. The efficiency of the internal conversion process increased, the efficiency of the light-emitting process decreased, and finally the fluorescence decreased. [20] In contrast, after doping with bpy to form Zn-bpy-HBPA, Zn²⁺ and HBPA were linked by bridging coordination to form the secondary building unit Zn-HBPA, Zn-HBPA were further linked by bpy into an one-dimensional infinite chain structure, then through the π - π stacking between the pyridine ring and the adjacent benzene ring, the one-dimensional chain structure formed a multi-dimensional structure. [21] On this basis, the N-substituted HBPA promotes the coplanarity of the aromatic substituent with the benzene ring, which could enhance and stabilize the delocalization (LLCT) state of the potential luminescent ligand-ligand transferred body, reduce the energy gap, and ultimately enhance the fluorescence performance.

Furthermore, on the basis of the above research, the influence of spraying times on the luminescence properties of Zn-HBPA@PFP and Zn-bpy-HBPA@PFP was studied. As shown in Fig. 7e and 7f, before responding to EtOH small molecules, the luminous intensity of Zn-HBPA@PFP and Zn-bpy-HBPA@PFP showed a trend of increases, then decreases with the change of spraying times, when Cycle=7 times, it had the best luminous intensity. After completing action on EtOH, Zn-HBPA@PFP showed a decrease tendency in fluorescence, while Zn-bpy-HBPA@PFP showed an increase tendency. Compared with the unresponsive result, the enhancement effect was still the best when Cycle=7 time. The experimental results displayed that MOFs@PFP had the maximum fluorescence intensity when sprayed for 7 times, which also showed that MOFs@PFP could be used as a flexible paper-based functional material that responds to EtOH small molecules.

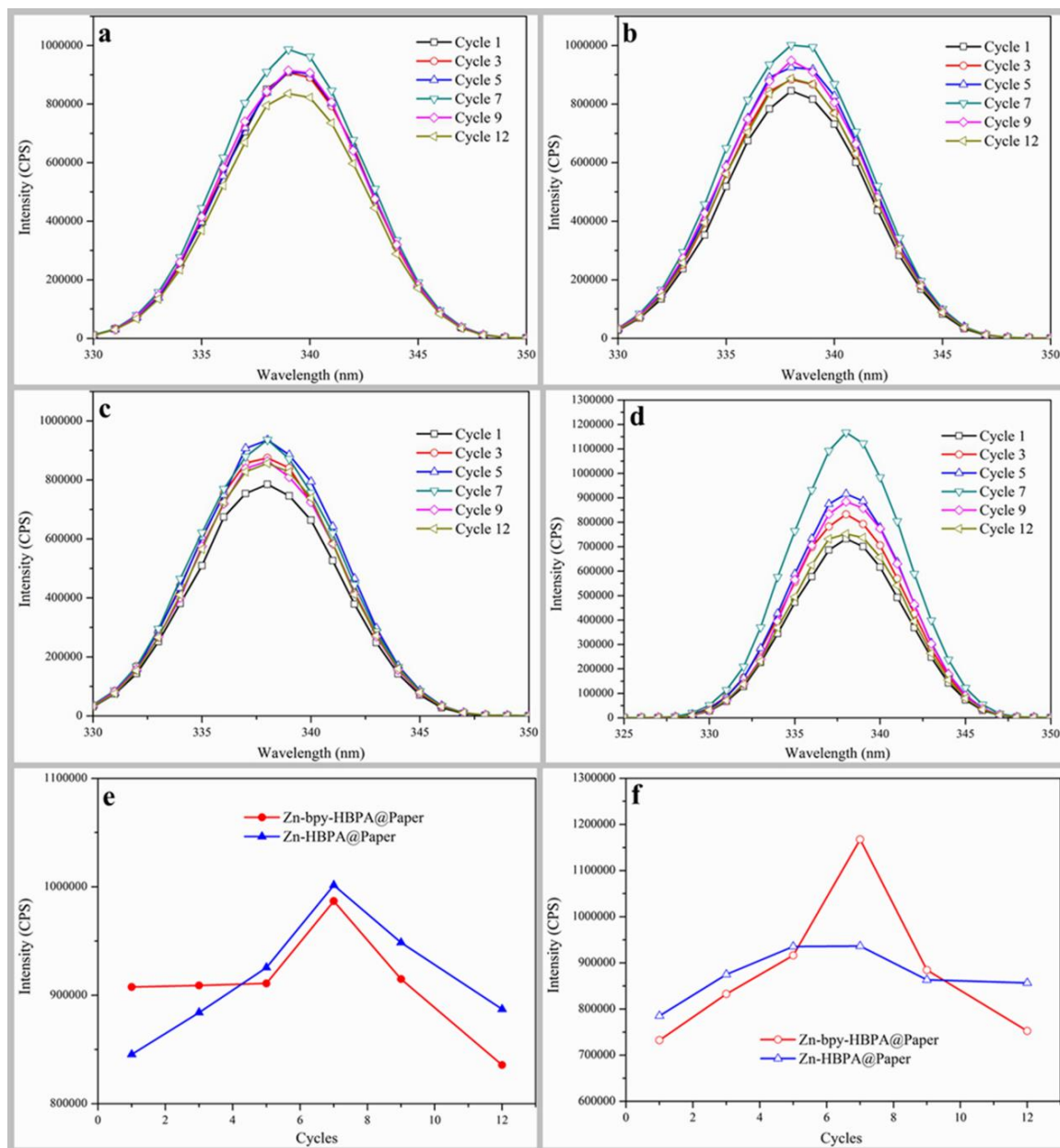


Fig. 7: The fluorescence responsivity curves of EtOH for Zn-HBPA@PFP and Zn-bpy-HBPA@PFP. (a) the fluorescence emission spectrums of normal Zn-HBPA@Paper; (b) the fluorescence emission spectrums of normal Zn-bpy-HBPA@Paper; (c) the fluorescence responsivity spectrums of Zn-HBPA@Paper; (d) the fluorescence responsivity spectrums of Zn-bpy-HBPA@Paper; (e) fluorescence contrast of MOFs@Paper at different spray times before response; (f) fluorescence contrast of MOFs@Paper at different spray times after response.)

Conclusion

- 1) A new type of organic ligand 3-(1-Oxo-1*H*-2,3-dihydroisoindol-2-yl)benzoic acid (HBPA) was synthesized, Zn-HBPA and Zn-bpy-HBPA with luminescent properties were prepared by

solvothermal method, the MOFs@PFP paper-based functional materials under different spraying times (Cycle=1, Cycle=3, Cycle=5, Cycle=7, Cycle=9, Cycle=12) were obtained by flame spraying. The FT-IR results showed that when Cycle=12 times, the infrared absorption of

MOFs reached the maximum, indicated that increased the number of spraying time could effectively improve the retention of MOFs on cellulose paper-based materials.

- 2) The fluorescence response of Zn-HBPA@PFP and Zn-bpy-HBPA@PFP to EtOH small molecules was investigated. The results showed that the luminous intensity of Zn-HBPA@PFP was reduced after ultraviolet light irradiation, which was manifested as a phenomenon of reduced fluorescence, while the luminous intensity of Zn-bpy-HBPA@PFP was increased, which was manifested as a phenomenon of increased fluorescence, indicated that after doping with 2,2'-bipyridine, the fluorescence response of MOFs@PFP to EtOH small molecules was significantly improved. In addition, research on the spraying process of MOFs@PFP showed that when the number of sprays was Cycle=7, Zn-bpy-HBPA@PFP had the best fluorescence enhancement effect.

Acknowledgements

We appreciate the financial which support from National Science Foundation of China (31670593), Basic Research Program of Natural Science of Shaanxi Province (2021JQ-839), Shangluo Science and Technology Plan Project (SK2018-03-02), Doctoral Scientific Research Foundation of Shang Luo University (18SKY003).

References

1. L. Liu, Z. B. Han, S. M. Wang, D. Q. Yuan, S. Ng, Robust Molecular Bowl-Based Metal–Organic Frameworks with Open Metal Sites: Size Modulation To Increase the Catalytic Activity, *Inorg Chem.*, **54**, 3719 (2015).
2. M. Ni, M. Gong, Li. X, J. Gu, Y. Chen, Dimensions of fluorescence kinetic concentration of doped morphology homologs synthesized by TCP and UiO-66 MOF, *Appl Mater Today.*, **23**, 100982 (2021).
3. J. G. Cheng, J. Liu, W. Q. Tong, D. Wu, Y. Y. Wang, Two new MOFs based on 5-((4-carboxypyridin-2-yl)oxy) isophthalic acid displaying unique selective CO₂ gas adsorption and magnetic properties, *Cryst Eng Comm.*, **21**, 7078 (2019).
4. H. R. Fu, Z. X. Xu, J. Zhang, Water-Stable Metal–Organic Frameworks for Fast and High Dichromate Trapping via Single-Crystal-to-Single-Crystal Ion Exchange, *Chem Mater.*, **27**, 205 (2015).
5. S. Yan, D. Deng, L. Zhang, Y. Lv, Fluorescence nano metal organic frameworks modulated by encapsulation for construction of versatile biosensor, *Talanta.*, **201**, 96 (2019).
6. J. N. Xiao, J. J. Liu, M. Y. Liu, G. F. Ji, Fabrication of a Luminescence-Silent System Based on a Post-Synthetic Modification Cd-MOFs: A Highly Selective and Sensitive Turn-on Luminescent Probe for Ascorbic Acid Detection, *Inorg Chem.*, **58**, 6167 (2019).
7. T. Alammar, I.Z. Hlova, S. Gupta, V. B. Lema, V. Pecharsky, A.V. Mudring, Luminescence properties of mechanochemically synthesized lanthanide containing MIL-78 MOFs, *Dalton T.*, **47**, 7594 (2018).
8. P. R. Matthes, F. Schönfeld, S. H. Zottnick, K. Müller-Buschbaum, Post-Synthetic Shaping of Porosity and Crystal Structure of Ln-Bipy-MOFs by Thermal Treatment, *Molecules.*, **20**, 12125 (2015).
9. Y. Ye, H. Liu, Y. Li, Q. Zhuang, P. Liu, J. Gu, One-pot doping platinum porphyrin recognition centers in Zr-based MOFs for ratiometric luminescent monitoring of nitric oxide in living cells, *Talanta.*, **200**, 472 (2019).
10. R. Hu, N. L. Leung, B. Z. Tang, AIE macromolecules: syntheses, structures and functionalities, *Chem Soc Rev.*, **43**, 4494 (2014).
11. N. B. Shustova, T. C. Ong, A. F. Cozzolino, V. K. Cozzolino, R. G. Griffin, M. Dinca, Phenyl Ring Dynamics in a Tetraphenylethylene-Bridged Metal–Organic Framework: Implications for the Mechanism of Aggregation-Induced Emission, *J Am Chem Soc.*, **134**, 15061 (2012).
12. D. L. Yang, X. Zhang, Y. G. Yao, J. Zhang, Structure versatility of coordination polymers constructed from a semirigid ligand and polynuclear metal clusters, *Cryst Eng comm.*, **16**, 8047 (2014).
13. Y. Sun, N. Ross, S. B. Zhao, K. Huszarik, W. L. Jia, Enhancing electron accepting ability of triarylboron via pi-conjugation with 2,2'-bipy and metal chelation: 5,5'-bis(BMes(2))-2,2'-bipy and its metal complexes, *J Am Chem Soc.*, **129**, 7510 (2007).
14. Q. Yang, W. Gong, X. W. Cui, C. S. Zhou, Functionalization of Cellulose Paper by Coating Nano Metal–Organic Frameworks for Use as Photochromic Material, *J.Chem.Soc.Pak.*, **43**, 67 (2021).
15. Q. Yang, M. Y. Zhang, S. X. Song, B. Yang, Surface modification of PCC filled cellulose paper by MOF-5 (Zn₃(BDC)₂) metal–organic

- frameworks for use as soft gas adsorption composite materials, *Cellulose.*, **24**, 1 (2017).
16. J. Y. Gao, N. Wang, X. H. Xiong, C. J. Chen, W. P. Xie, X. R. Ran., Y. Long, S. T. Yue, Y. L. Liu, Syntheses, structures, and photoluminescent properties of a series of zinc(II)-3-amino-1,2,4-triazolate coordination polymers constructed by varying carboxylate anions, *Cryst Eng comm.*, **15**, 3261 (2013).
 17. Y. Chen, H. Li, S. Cai. Luminescent N-arylphthalimidino derivatives 2-and 4-(1-oxo-1H-2,3-dihydroisoindol-2-yl)benzoic acid: examples of a new class of reaction induced crystallization for an organic compound, *Chem Comm.*, **36**, 5392 (2009).
 18. R. P. Ye, X. Zhang, J. Q. Zhai, J. Zhang, N-donor ligands enhancing luminescence properties of seven Zn/Cd(II) MOFs based on a large rigid π -conjugated carboxylate ligand, *Cryst Eng Comm.*, **17**, 9155 (2015).
 19. N. Barman, D. Singha, K. Sahu. Fluorescence quenching of hydrogen-bonded coumarin 102-phenol complex: effect of excited-state hydrogen bonding strength, *J Phys Chem A.*, **117**, 3945 (2013).
 20. L. Wang, Y. Wang, Q. Zhang, J. Zhao, Theoretical exploration about the ESIPT mechanism and hydrogen bonding interaction for 2-(3,5-dichloro-2-hydroxy-phenyl)-benzoxazole-6-carboxylic acid, *J Phys Org Chem.*, **33**, 145 (2020).
 21. D. H. Hu, C. Y. Sun, F. H. Liu, C. Qin, X. L. Wang, Z. M. Su, A series of coordination complexes based on unsymmetrical multicarboxylate ligands: syntheses, structures and properties, *Cryst Eng comm.*, **15**, 6769 (2013).